

# Mode II fracture toughness of asymmetric metal-composite adhesive joints

Panayiotis Tsokanas<sup>1</sup>, Theodoros Loutas<sup>1,\*</sup>, Dimitrios Pegkos<sup>1</sup>, George Sotiriadis<sup>1</sup>, and Vassilis Kostopoulos<sup>1</sup>

<sup>1</sup>Laboratory of Applied Mechanics and Vibrations, Department of Mechanical Engineering and Aeronautics, University of Patras, Patras University Campus, GR-26504 Rio-Patras, Greece

**Abstract.** The paper presents an experimental investigation of the mode II fracture toughness behavior of dissimilar metal-composite adhesive joints using the end-notched flexure (ENF) test. The adhesive joint under study consists of a thin titanium sheet joined with a thin CFRP laminate and is envisioned to be applied in the hybrid laminar flow control system of future aircraft. Four different industrial technologies for the manufacturing of the joint are evaluated; co-bonding with and without adhesive and secondary bonding using either a thermoset or a thermoplastic composite. The vacuum-assisted resin transfer molding (VARTM) technique is employed for the manufacturing of the titanium-CFRP joint. After manufacturing, the joint is stiffened from its both sides with two aluminum backing beams to prevent large deformations during the subsequent ENF tests. Towards the fracture toughness determination from the experimental data, an analytical model recently reported by the authors is applied; that model considers the bending-extension coupling of each sub-laminate of the joint as well as the effect of the manufacturing-induced residual thermal stresses. The load-displacement behaviors, failure patterns, and fracture toughness performances for each of the four manufacturing options (MO) investigated are presented and compared.

## 1 Introduction

Dissimilar adhesive joints are finding increasing usage in many high-performance structural applications in several industries (e.g. aerospace, automotive, wind energy, etc.). A common combination of dissimilar materials in many industries are metals (aluminum, steel, titanium, etc.) and composites (CFRP, GFRP, etc.); a very typical example are the fiber metal laminates (FML).

The last decades, intense scientific interest has been expressed towards the experimental investigation and characterization of the quasi-static mode I, mode II, and mixed-mode I/II interfacial fracture toughness of structural adhesive joints consisting of either *similar* (e.g. metal-metal or composite-composite) or *dissimilar* (e.g. metal-composite) adherents. A review of the related literature is presented in our previous paper [1]. Among this literature

---

\* Corresponding author: [thloutas@upatras.gr](mailto:thloutas@upatras.gr)

though, the works using the ENF configuration, and especially for the analysis of dissimilar metal-composite adhesive joints, are rare (see e.g. [2, 3]).

The present work builds on previous research [1, 4, 5] by the group. Here, the quasi-static mode II fracture toughness behavior of adhesively bonded joints between titanium and carbon-epoxy composite adherents under ENF loading is experimentally investigated. The joint configuration studied is uncommon; the titanium and composite adherents have different thicknesses, while also two aluminum backing beams were applied in both sides of the titanium-CFRP joint to prevent large deformations of the adherents during the subsequent tests. More information about the design and the intended application of the joint in future aircraft is found in our previous work [4]. Four different technologies (so-called MO) have been considered for the joining of the titanium and CFRP; namely co-bonding with and without adhesive, secondary bonding using thermoset composite and secondary bonding using thermoplastic composite. The previous paper [1] details the manufacturing processes. After manufacturing, quasi-static ENF tests were performed at room temperature conditions and as close to the AITM standard as possible. Fractographic analyses were undertaken to extract the failure modes. The analytical model presented in [6] was used for the calculation of the strain energy release rates (SERR) and mode mixities of the ENF tests. The four MO used were compared in terms of their load-displacement responses, failure patterns, and SERR performances.

## **2 Experimental methods**

### **2.1 The metal-composite adhesive joint**

We investigate the mode II fracture toughness of the adhesive joint shown in Figure 1, whose both titanium and CFRP adherents are very thin. In our previous paper [4], the issue of design of interfacial fracture toughness tests for this joint, as well as the envisioned aerospace application of the joint, are covered. The joint is stiffened from both titanium and CFRP sides with two aluminum beams, as shown in Figure 1a. Before stiffening, the joining of the titanium with the composite was performed at high temperature (see Paragraph 2.2), which induces high residual thermal stresses after joining. In the present work, the backed joint with residual thermal stresses is experimentally studied using the ENF tests. Last, the four MO outlined in Figure 1b are evaluated.

### **2.2 Materials and manufacturing processes**

The information on the materials used is given in [1]. In Figure 1b, the materials and stacking sequences of the CFRP laminates, as well as the applied curing temperatures are presented. In Table 1, the mechanical properties, physical properties, and thicknesses of the joint's constituent materials are listed. The manufacturing processes of the ENF test specimens were identical with the ones presented in [1] for the double cantilever beam (DCB) ones.

### **2.3 End-notched flexure (ENF) experiments**

The quasi-static mode II interfacial fracture toughness experiments, using the ENF configuration, were performed at room temperature conditions (25 °C and 50-60% RH) using a 25 kN Instron universal testing machine (Instron, High Wycombe, UK). The experiments were conducted as close as possible to the AITM 1.0006 standard's guidelines.

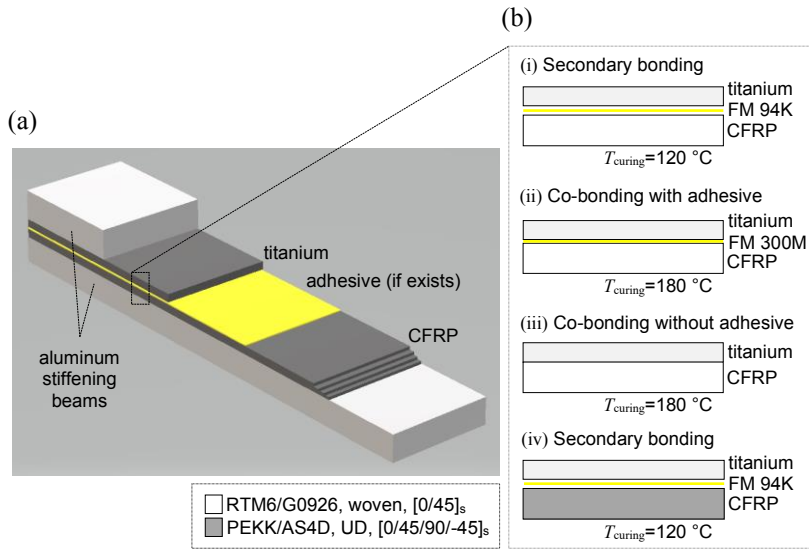


**Fig. 1.** The under-investigation titanium-CFRP adhesive joint. (a) The sequence of the individual layers comprising the adhesive joint, after the addition of the aluminum stiffening beams. (b) Schematic representation of the four manufacturing options (MO) studied; (i) MO 1, (ii) MO 2, (iii) MO 3, and (iv) MO 4.

The experimental setup for the ENF tests is schematically shown in Figure 2. The dimensions of the ENF specimens, namely the width  $b$ , span length  $L$ , initial crack length  $a_0$ , and sub-laminates' thicknesses  $h_1$  and  $h_2$ , are shown in this figure. The values of  $b$ ,  $L$ , and  $a_0$  are given in Table 2.

During the ENF tests, the crosshead displacement rate was fixed at 1 mm/min. Also, the applied load  $P$  and crosshead displacement  $\delta$  of the test machine were continuously recorded during the test. The  $P$  versus  $\delta$  curves were registered and used for the determination of the fracture toughness of the joint. A minimum of three specimens for each MO was tested.

**Table 1.** Elastic properties, physical properties, and nominal thicknesses of the materials of the titanium-CFRP adhesive joint.

Material	$E_1$ (GPa)	$E_2$ (GPa)	$G_{12}$ (GPa)	$\nu_{12}$ (-)	CTE $a_1, a_2$ ( $\cdot 10^{-6}/^{\circ}\text{C}$ )	Thickness (mm)
Titanium	105.0	105.0	45.0	0.340	8.6	0.800
CFRP, woven <sup>1</sup>	66.0	66.0	4.5	0.035	2.9	0.363
CFRP, UD <sup>1</sup>	139.0	10.5	5.2	0.076	1.0	0.140
Aluminum	73.1	73.1	28.0	0.330	-	5.000

<sup>1</sup> The given properties and thicknesses refer to the level of layer  
 CTE: coefficient of thermal expansion

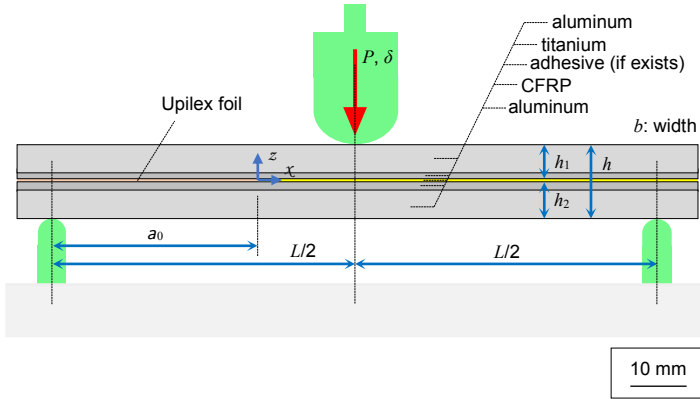


**Fig. 2.** Experimental setup (in scale) for the end-notched flexure (ENF) experiments.

## 2.4 Experimental data reduction

Owing to difficulties in defining the exact crack initiation load ( $P_{ini}$ ) in the ENF tests, the non-linearity criterion, defining the crack initiation at the point where the load versus displacement trace deviates from linearity, is used here for the estimation of the  $P_{ini}$ .

Next, the analytical model proposed in [6] is utilized in order to estimate the total SERR, as well as the “parasitic” mode mixity, at  $P_{ini}$ . As it is evident, the present joint consists of two *sub-laminates* that exhibit bending-extension coupling as well as they contain residual thermal stresses; the analytical model of [6] considers both of these effects.

The model is schematically shown in Figure 3. We consider a laminated cantilever beam, having an asymmetric delamination, being end-loaded with vertical forces, and containing residual thermal stresses. The interfacial crack lies along the interface of the upper sub-laminate (sub-laminate 1) and the lower sub-laminate (sub-laminate 2), both of which are modeled as shear-deformable, elastic, and generally layered beams.

**Table 2.** Dimensions of the end-notched flexure (ENF) test configurations.

MO	$b$ (mm)	$L$ (mm)	$a_0$ (mm)
1	25	120	35
2	25	120	35
3	25	100	35
4	25	120	35

MO: manufacturing option

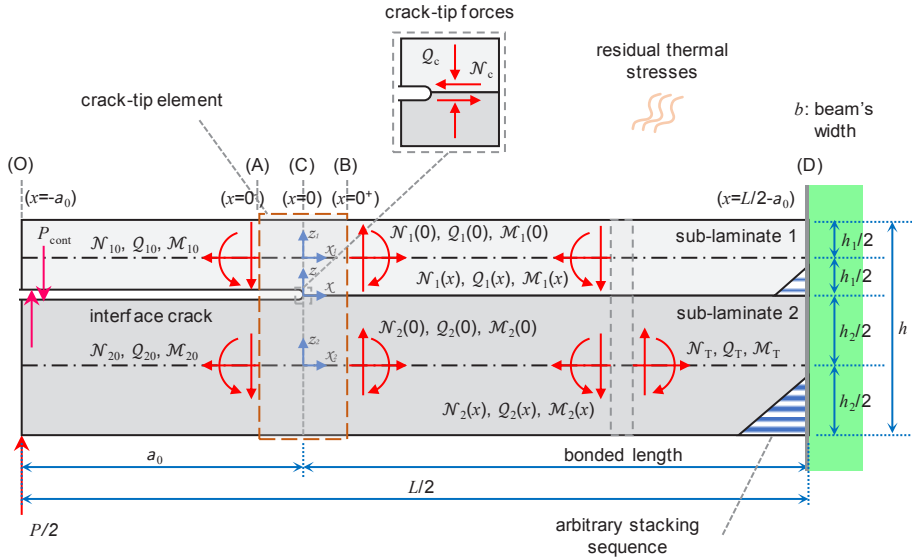


**Fig. 3.** Schematic of the beam model [6] used for the determination of the fracture toughness of the titanium-CFRP adhesive joint using the end-notched flexure (ENF) configuration. An elastic, laminated, and cantilever beam, consisting of two sub-laminates with arbitrary stacking sequences and an asymmetric through-the-width interfacial disbonding (crack), is end-loaded with concentrated vertical forces ( $P/2$  and  $P_{\text{cont}}$ ), as well as it contains manufacturing-induced residual thermal stresses.  $P_{\text{cont}}$  is the contact force between the upper and lower unbonded arms of the beam.  $b$ ,  $L/2$ , and  $a_0$  are the width (not shown in the figure), total length, and initial crack length of the beam, respectively.  $h_i$ ,  $i=1, 2$ , is the thickness of the sub-laminate  $i$ .  $N_c$  and  $Q_c$  are the crack-tip forces. The internal forces and moment,  $N_i$ ,  $Q_i$ , and  $M_i$ ,  $i=1, 2$ , developed at various cross-sections of the beam, are shown in the figure.

Following the Irwin approach, the mode I, mode II, and total SERR can be expressed in terms of the crack-tip forces  $N_c$  and  $Q_c$  shown in Figure 3, and two coefficients called *flexibility coefficients*. These coefficients consist measures of the elastic deformability of the crack-tip element. For the ENF configuration, the SERR are the following [6]:

$$G_I = \frac{1}{2} (c_1 + c_2) \left\{ P_{\text{cont}}(1 + \lambda a_0) - \frac{P}{2}(1 + \lambda a_0) \frac{2d_2\eta + (h_1 + h_2)d_2\xi + 2b_2\xi}{2(d_1 + d_2)\eta + [2b_1 + 2b_2 + (h_1 + h_2)d_2]\xi} + \frac{2\lambda\xi [\alpha_{N2} - \alpha_{N1} + \frac{\eta}{\xi}(\alpha_{M2} - \alpha_{M1}) + \frac{h_1 + h_2}{2}\alpha_{M2}]^2}{2(d_1 + d_2)\eta + [2b_1 + 2b_2 + (h_1 + h_2)d_2]\xi} \right\}^2$$

$$G_{II} = \frac{1}{2} \left( a_1 + a_2 - h_1b_1 + h_2b_2 + \frac{h_1^2}{4}d_1 + \frac{h_2^2}{4}d_2 \right) \left\{ \frac{2}{h_1\xi + 2\eta} \left[ \xi P_{\text{cont}} + \left( b_2 + \frac{h_2}{2}d_2 \right) \frac{P}{2} \right] a_0 - \alpha_{N1} + \alpha_{N2} + \frac{h_1}{2}\alpha_{M1} + \frac{h_2}{2}\alpha_{M2} \right\}^2 \quad (1)$$

$$G = G_I + G_{II}$$

In Eqs. (1),  $G_I$ ,  $G_{II}$ , and  $G$  are the mode I, mode II, and total SERR.  $P_{\text{cont}}$  is the contact force between the upper and lower unbonded arms (see Figure 3). The elastic constants  $a_i$ ,  $b_i$ ,  $c_i$ , and  $d_i$ ,  $i = 1, 2$ , are the *extensional compliance*, *bending-extension coupling compliance*, *shear compliance*, and *bending compliance*, respectively, of the sub-laminate  $i$ .  $\alpha_{Ni}$  and  $\alpha_{Mi}$ ,  $i = 1, 2$ , are the *axial strain* and *curvature* of the sub-laminate  $i$  due to residual thermal stresses.  $\lambda$ ,  $\xi$ , and  $\eta$  are auxiliary parameters.

### 3 Results and discussion

#### 3.1 Load-displacement responses

In Figure 4, the load versus displacement curves from the ENF experiments of all MO are shown. Every curve corresponds to one successful experiment while the four different diagrams serve to compare the fracture behaviors of the four different MO studied.

In general, there are three phases in the curves of all diagrams; (a) phase 1: the evolution of the curve and thus of the material behavior is linear; (b) phase 2: loss of linearity, that implies the appearance of some irreversible processes, probably in the interface layer (plasticity or damage); and (c) phase 3: the load drops, which corresponds to crack propagation. In the curves of all MO, and especially in those of MO 1, 2, and 4, the load drop is relatively “smooth”, implying a gradual degradation of material property.

The  $P_{ini}$  cannot be obvious on the curves of Figure 4. Nevertheless, a good estimation of that point was made by applying the non-linearity criterion; the resulting  $P_{ini}$  values are shown in Table 3.

#### 3.2 Fractographic analysis

After the tests, the fracture surfaces of the specimens were examined using a high-resolution digital camera in order to assess the causes of failure (Figure 5). The classification of the involved failure modes was performed in accordance with the ASTM D5573 standard. The three failure modes observed are (a) adhesive failure, (b) cohesive failure, and (c) thin-layer cohesive failure. Between them, the dominant is the third one for all MO.

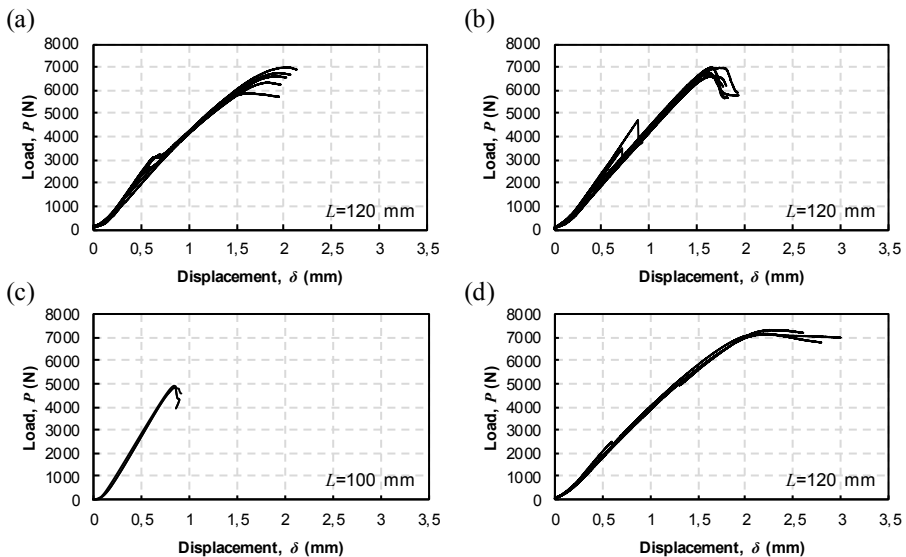


**Fig. 4.** Load ( $P$ ) versus crosshead displacement ( $\delta$ ) curves during the end-notched flexure (ENF) experiments, for the four manufacturing options (MO) studied, the (a) MO 1, (b) MO 2, (c) MO 3, and (d) MO 4.  $L$  is the span length of the ENF configuration.

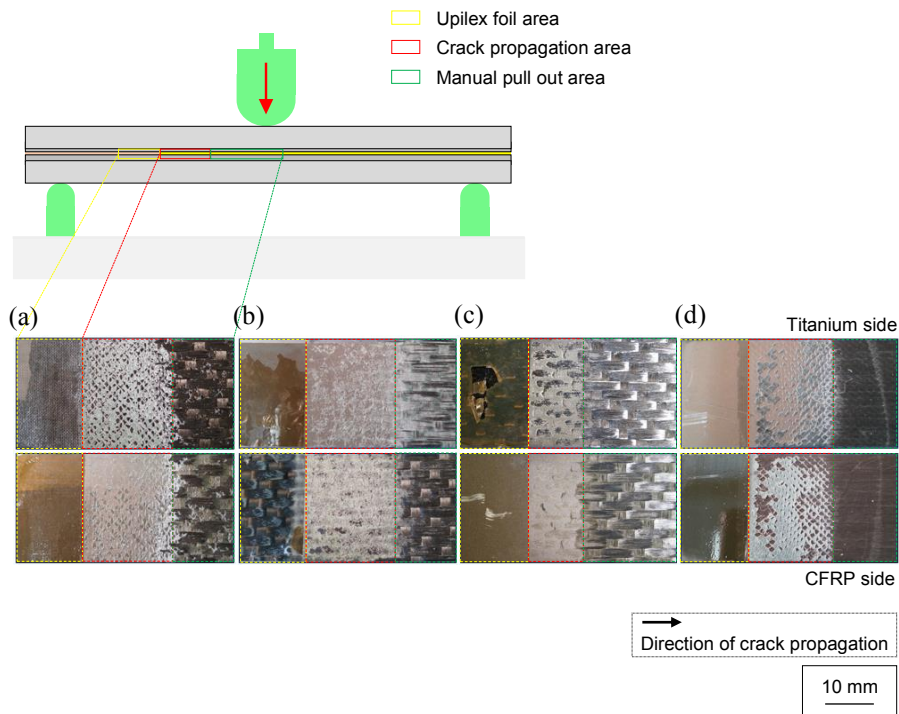


**Fig. 5.** Fracture surfaces of a representative end-notched flexure (ENF) specimen from each of the four manufacturing options (MO) studied. (a) MO 1. (b) MO 2. (c) MO 3. (d) MO 4.

### 3.3 Strain energy release rates (SERR) and mode mixities

The total SERR and “parasitic” mode mixities at  $P_{ini}$ , calculated using the data reduction scheme of [6], are presented in Table 3 for all MO. As shown in this table, in terms of the total SERR, the best and worst performing MO are the MO 4 and 3, respectively. For all MO, the mode mixity at  $P_{ini}$  is practically negligible (lower than 1%).

**Table 3.** Strain energy release rate (SERR) ( $G$ ) and mode mixity ( $G_I/G$ ) values for all manufacturing options (MO).

MO	Load, $P_{ini}$ (N)	SERR, $G$ (N/m)	Mode mixity, $G_I/G$ (%)
1	6002.0 ( $\pm 209.8$ )	2360.0 ( $\pm 154.7$ )	0.5
2	6550.0 ( $\pm 202.5$ )	2666.7 ( $\pm 188.1$ )	0.1
3	4633.3 ( $\pm 102.7$ )	1296.0 ( $\pm 61.2$ )	0.0
4	6475.0 ( $\pm 309.2$ )	2819.8 ( $\pm 285.5$ )	0.9

MO: manufacturing option. SERR: strain energy release rate

## 4 Summary and conclusions

We have presented an experimental investigation of the mode II interfacial fracture toughness of an adhesive joint between titanium and CFRP. The industrial end-user (i.e. Aernnova) of the joint required that the adherents' thicknesses are very small. Based on this, aluminum backing beams were added to avoid large deformations of the adherents during testing and extract correct fracture toughness properties. Four different MO were investigated using cost-effective industrial manufacturing processes. These processes were co-bonding with and without adhesive and secondary bonding using either a thermoset or a thermoplastic composite. The evaluation of these MO was performed using ENF experiments. An analytical model recently developed by the authors, that considers the bending-extension coupling of both sub-laminates of the joint as well as the manufacturing-induced residual thermal stresses effect, was applied for experimental data reduction.

The main conclusions arising from the present study are the following:

- The three failure modes observed are adhesive failure, cohesive failure, and thin-layer cohesive failure. Between them, the dominant is the third one for all MO.
- Regarding the total SERR at  $P_{ini}$ , the MO 4 is the best performing one. Based on the utilized data reduction scheme, it achieves a SERR value of 2820 N/m while the worst one MO, the MO 3, reaches a SERR value of 1296 N/m.
- The “parasitic” mode mixity that is introduced in the ENF tests due to the asymmetry of the joint as well as the presence of residual thermal stresses, is for all MO negligible at  $P_{ini}$  (lower than 1%).

It should be noted that, due to length restrictions, the present paper is a brief version of a more detailed work to be reported by the authors in near future.

The work presented in this paper was financially supported by the Clean Sky 2 Joint Undertaking under the European Union's Horizon 2020 research and innovation program TICOAJO (Grant Agreement Number: 737785). The support is appreciated by the authors. Also, the authors thank their TICOAJO partners from the Royal Netherlands Aerospace Centre (NLR), The Netherlands, and especially Mr. W.M. van den Brink and Mr. P. Nijhuis, for performing the manufacturing of the test specimens. Finally, the authors thank their TICOAJO partners from the Structural Integrity and Composites (SI&C) research group, Delft University of Technology, The Netherlands, and especially Dr. W. Wang, Dr. J.A. Poulis, Prof. S. Teixeira De Freitas, and Prof. D. Zarouchas, for performing the surface pre-treatment studies.

## References

1. T. Loutas, P. Tsokanas, V. Kostopoulos, P. Nijhuis, W.M. van der Brink, Mater. Today-Proc. (to be published)
2. M.F.S.F. de Moura, R.D.S.G. Campilho, J.P.M. Gonçalves, Int. J. Solids Struct. **46**, 1589 (2009)
3. C. Alía, J.M. Arenas, J.C. Suárez, R. Ocaña, J.J. Narbón, J. Adhes. Sci. Technol. **27**, 2480 (2013)
4. P. Tsokanas, T. Loutas, V. Kostopoulos, Y. Essa, F.M. de la Escalera, In Proc. 18<sup>th</sup> Eur. Conf. on Composite Materials, 2018
5. P. Tsokanas, T. Loutas, G. Kotsinis, In Proc. 7<sup>th</sup> ECCOMAS Thematic Conf. on the Mechanical Response of Composites, 2019
6. P. Tsokanas, T. Loutas, Eng. Fract. Mech. **214**, 390 (2019)